MEASUREMENT OF ROTOR BLADE STRUCTURAL DYNAMICS

Simone Weber
Airbus Helicopters UK
Cranfield University, UK

Thomas Kissinger, Edmond Chehura, James Barrington, Stephen Staines, Mudassir Lone, Stephen James and Ralph Tatam
Cranfield University, UK

Abstract
Initial results collected with optical fibre Bragg grating (FBG) strain sensors and with a novel direct fibre optic shape sensing approach during a series of ground vibration tests performed on a rotor blade are presented. A number of key benefits highlight the potential of applying the shape sensing system to complex rotor blade structures: (1) no information of the underlying structure is required to infer the shape and (2) the rotor blade structural characterization can be achieved with only one straight fibre optic cable that is mounted along the length of a rotor blade. An assessment of sensor performance has shown that the results are within 4% agreement with commercially available instrumentation systems. Limitations of the use of FBG based strain gauges are discussed in terms of the dependency of strain measurements on the position of neutral axis.

1. INTRODUCTION

The helicopter design and engineering community is fully aware of the complex dynamic behaviour of rotor blades, and as a result has established design processes and guidelines that are used in technical domains ranging from design all the way to maintenance. This understanding has led to fundamental shifts in designs where, instead of physical flapping and torsional hinges such as that on the Sikorsky S-58, modern rotorcraft have these hinges fully incorporated within a single composite flexbeam. Moreover, the multi-role nature of helicopter operations means that the rotorblades are required to perform over a very broad flight envelope and consequently today's rotorblade designs have evolved to have very complex, light weight internal structures. Overall, these factors lead to a series of challenging problems in the development of model based design methods and in the development of validation techniques. In this paper, the authors discuss the work carried out within the BladeSense project that aims to use state-of-the-art instrumentation on an Airbus Helicopters H135 rotorblade to collect experimental blade deformation data.

The paper will be structured such that the foundations of the structural modelling approach is presented first. This will describe the development of one-dimensional beam elements coupled with scalar spring elements to represent the complex interconnection of the pitch control cuff and flexbeam to model the bearingless main rotor. The structural dynamics model is coupled to surface points representing the blade's geometric surface. Issues such as the accurate measurement and prediction of surface strain will be discussed in the context of limitations due to lack of information regarding the neutral axis of the blade. This will be followed by an overview of the instrumentation deployed on the blade. The blades have been instrumented using two types of fibre optic sensors: (1) multiplexed arrays of fibre Bragg gratings (FBG) that act as strain gauges and (2) a novel method that allows he direct measurement of shape. The advantage of this novel approach is that it does not require perfect strain transfer from the structure to the sensing fibre, but only needs the optical fibre to follow the structure through space. The use of FBG strain sensors together with accelerometers (ACC) allows the novel shape sensing technique to be validated. A preliminary assessment of sensor performance has been carried out via a series ground vibration tests using a full scale H135 rotorblade. Modal parameters obtained from each set of sensors are compared against each other, highlighting the suitability of the use of fibre optic sensors to capture the dynamics of such complex structures.
The paper concludes by comparing the structural model with modal parameters obtained from analysis of the experimental data.

2. STRUCTURAL MODEL DEVELOPMENT

The bearingless main rotor (BMR) of a H135 is characterised by the lack of mechanical flapping, lagging, and torsional hinges. Instead, these are incorporated in the design of the flexbeam by varying the geometrical cross-sections and material properties. Detailed information about the H135 can be found in References [1] [2] [3].

The finite element (FE) analysis model of the H135 rotor blade was constructed using standard finite-element-modelling techniques in Nastran. This

Presented at 44th European Rotorcraft Forum, Delft, The Netherlands, 19-20 September, 2018

software seemed to be suited for this task due to the available data format of material and cross-sectional properties for a large number of structural nodes. This data was given as a product of material properties and moment of inertia of the geometrical area, such as EIx, EIy, or torsional rigidity GJ. Although the material properties vary along the rotor radius, it is assumed that these remain constant between the structural nodes. The schematic of the one-dimensional modelling principle is shown in Figure 1. The structure of the rotor blade is modelled using multiple beams that consist of a primary one-dimensional stick for the flexbeam and the blade aerofoil section, and a secondary stick parallel to the flexbeam representing the pitch control cuff. Scalar spring elements are incorporated to ensure a correct coupling between the flexbeam and pitch control cuff, and to take into account the stiffness of the rotational movement induced by the pitch control cuff.

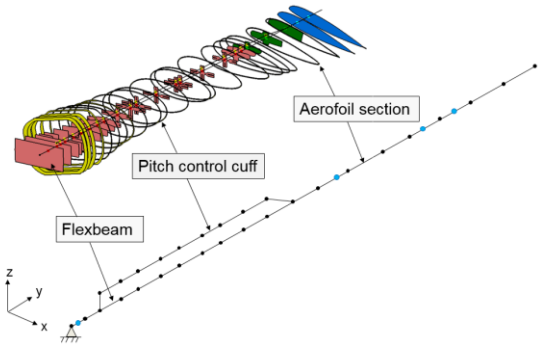

Figure 1: Structural main rotor blade model

Coupling the structural dynamics model to surface points representing the blade's geometric surface is necessary, as the sensors are placed on the surface during structural testing. This task is simplified by the use of only two geometrical profiles for the cuff and blade profile, which are then scaled according to the spanwise thickness to chord ratio. With the use of transformation matrices, the profiles are rotated around the structural centre. It is assumed that the shape of the cross-section remains unaltered during deformation, regardless of the loading conditions. Warping and shear deformations of the blade profile are neglected.

The non-rotating natural frequencies and mode shapes were produced using the Nastran modal analysis solver. The mode shapes can be visually represented with the use of the geometrical blade profiles. Figure 2 shows the first eight structural mode shapes of the rotor blade. While the first four mode shapes have a dominant flapping or lagging component, the 5th mode shape exhibits a coupled flapping/lagging part, the 6th mode shape has a coupled torsion/flapping component, and the 7th mode has a coupled lagging/flapping part. This coupling occurs mainly due to the chord-wise locations of the centre of gravity and shear centre [4].

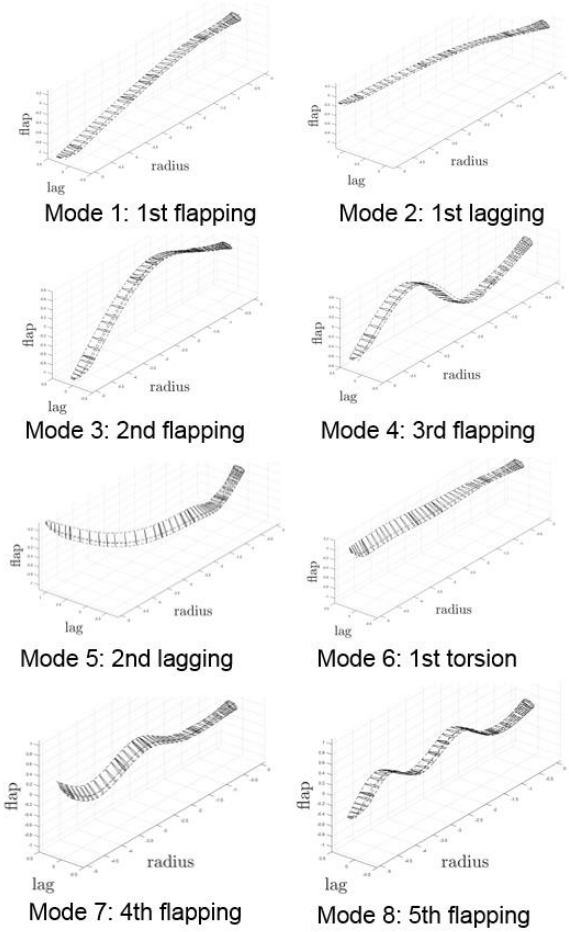

Figure 2: Mode shapes

With the use of a finite number of displacement and strain mode shapes, the displacement and strain of the structure can be approximated. This is achieved by the summation of their mode shapes that are weighed by the corresponding generalised coordinates f_i:

(1) $$d(x,y,z,t) = \sum_{i=1}^{n} \phi_i(x,y,z) f_i(t)$$

(2) $$\epsilon(x,y,z,t) = -c(x,z) \sum_{i=1}^{n} \psi_i(x,y,z) f_i(t)$$

Where d and ϵ are the displacement and strain functions at any point along the entire rotor blade, and n is the number of modes used. ϕ_i and ψ_i are the *i*th displacement and *i*th strain mode shape, respectively. The strain mode shape ψ_i is expressed as the second spatial differential with respect to spanwise direction y:

(3) $$\psi_i = \frac{\partial^2 \phi_i}{\partial y^2}$$

Presented at 44th European Rotorcraft Forum, Delft, The Netherlands, 19-20 September, 2018

The strain is dependent on $c(x,z)$, which is the distance between neutral axis and surface. The lack of information of the exact position of the neutral axis leads to assumptions being made for the strain calculation. This consequently leads to uncertainties in the mathematical model description. Figure 3 shows an example of the assumed location of neutral axis for the used aerofoil and pitch control cuff. The position varies along the length of the rotor blade, but it is close to the quarter chord line. The same is valid for the pitch control cuff, although at radial sections where the pitch control cuff has a symmetric shape the neutral axis is assumed to be at its centroid position. To calculate surface strain due to out-of-plane or in-plane bending, the distance between neutral axis and surface needs to be defined in both directions.

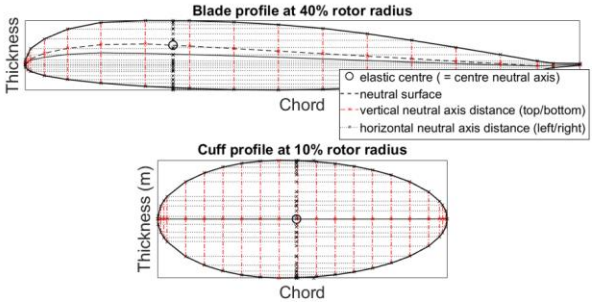

Figure 3: Definition of neutral axis position

It should be noted that the uncertainty of the neutral axis location is not the only contribution to the total surface strain error, as the simplifications made for the structural model using two different geometrical profiles for the entire rotor blade also contribute. Therefore, experimental testing is a critical task, not only for model validation but also to extract correction factors for the strain calculation from the test results.

3. OVERVIEW OF USED INSTRUMENTATION SYSTEM

The rotor blade was instrumented using five uni-axial accelerometers and two optical fibre sensing technologies: FBGs and direct fibre optic shape sensing (DFOSS). The accelerometer data, together with that from the FBGs, were used as the baseline for data comparison.

Optical fibre based sensing approaches have been adopted here as they offer a number of key benefits, including their flexibility, low weight, electromagnetic immunity, small dimensions (~0.2 mm diameter), no requirement for electrical connection to the sensing elements and the ability to multiplex a number of sensors within a single length of optical fibre. In addition, optical fibres can be embedded within fibre reinforced composites during fabrication, or, alternatively, can be surface-mounted to facilitate retrofitting [5] [6] [7].

FBGs represent a mature sensing technology that is commercially available. An FBG is a method for labelling a short section of optical fibre (of length typically 0.5 – 5 mm) such that it can be uniquely interrogated to monitor local environmental parameters such as strain and temperature [8]. The label takes the form of a grating structure that is created within the core of the optical fibre by exposure of the fibre to a spatially modulated UV laser beam. The grating acts as a wavelength selective mirror, reflecting a single wavelength of light back along the optical fibre. Perturbation of the grating by strain or temperature results in a change in the reflected wavelength, the measurement of which forms the basis of the sensing approach. It is possible to multiplex a number of such sensors within a single optical fibre by fabricating each FBG such that in their quiescent states they each reflect different wavelengths. Typical commercially available sensor interrogation units (which can be flight-certified) are capable of performing measurements of strain and temperature with resolutions of 1 με and 0.1 K, respectively, in 4 - 16 fibres, with tens of sensors per fibre, at data rates up to 100 kHz (typically of order 1 kHz). In this application, arrays of FBG strain sensors, attached to the upper and lower surface of the blade, will be used to measure the vibration mode shapes indirectly, where the data has to be combined with a model of the blade to determine the shape from the measured strain [9].

DFOSS allows changes in the fibre path, and thus changes in the shape of the structure to which the fibre is attached, to be followed in three dimensions. A key advantage of DFOSS is that the shape is determined directly within the sensing fibre, removing the dependence on strain transfer from the structure and thus the requirement for a model of the structure. Simple surface mounting of the sensing fibre, for example using adhesive tape, is, in principle, sufficient. The DFOSS approach proposed here [10] is based on Fibre Segment Interferometry, an approach pioneered at Cranfield University [11] [12], which employs a simple, cost-effective and robust interrogation system exploiting well-proven telecoms laser diodes, detectors and optical fibre components to offer highly sensitive high-speed dynamic curvature measurements. The approach relies on differential measurements of strain in fibre segments formed in the cores of a multi-core optical fibre, with the segments bounded by low reflectivity, broad bandwidth FBGs.

Presented at 44th European Rotorcraft Forum, Delft, The Netherlands, 19-20 September, 2018

4. EXPERIMENTAL TESTING

A ground vibration test (GVT) has been carried out by exciting the rotor blade with the use of a random-on-random (RoR) vibration control in a frequency range of 0-100 Hz. The test bench consists of a rig designed for mounting the rotor shaft and rotor blade as shown in Figure 4. The excitation was introduced to the rotor blade through a shaker via a stinger that was attached to the pitch control cuff.

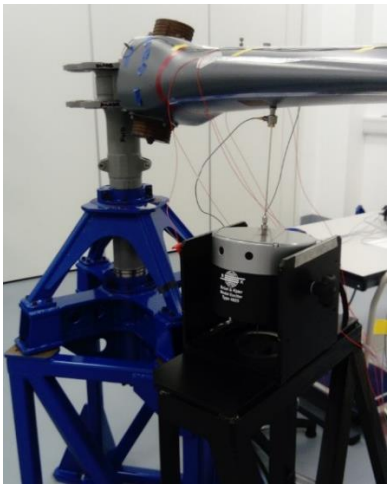

Figure 4: Ground vibration test set-up

Figure 5 shows the instrumentation set-up comprising accelerometers, FBG arrays and the shape sensing cable.

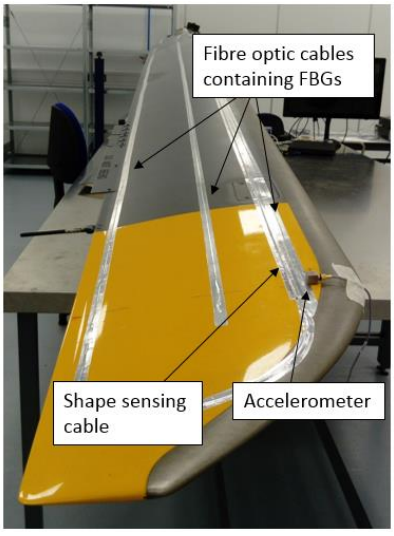

Figure 5: Instrumentation set-up

The five accelerometers, as well as the shape sensing system, were located along the aerofoil quarter chord line. In total, six fibre optic cables with each containing nine wavelength-division-multiplexed FBGs, were mounted on the top and bottom surfaces of the rotor blade. As shown in Figure 5 the fibre optic cables are located close to the leading edge at the quarter chord line, at the half chord position, and close to the trailing edge.

The FBGs reflecting in the wavelength band 1528-1568 nm were fabricated in hydrogen loaded SMF-28 optical fibres. The FBGs were attached to the blade using a cyanoacrylate adhesive and protected with a capping layer of 2-part epoxy. Correct bonding is important for appropriate strain transfer from the structure to the sensor. In order to protect the fibre optic cables, strips of aluminum speed tape covered the length of the FBG arrays.

The DOFSS system comprised three optical fibres mounted on a 3D printed support structure. Each fibre contained seven sensing sections, of length 600mm, formed between eight low reflectivity broadband Bragg reflectors. The support structure was designed to hold the fibres such that changes in the shape of the structure in two dimensions perpendicular to the fibre resulted in differential strains between the fibres, from which the shape of the structure can be determined. The support structure was secured on the upper surface of the blade using aluminium speed tape.

5. DATA ANALYSIS AND COMPARISON

The performance of the DOFSS system can be assessed by comparing the measurements with data obtained from the the accelerometers and FBGs. During the GVT, each acquisition system recorded the structural response in time.

Before the FBG data could be analysed, the recorded wavelength change from each FBG was converted to micro strain $\mu\epsilon$ using the following equation:

$$\mu\epsilon_i = \Delta\lambda f \tag{4}$$

Where $\Delta\lambda$ is the wavelength change in nano-meters, and f is the FBG wavelength strain coefficient, usually assumed to be 1.2 [13].

A fast Fourier transform (FFT) algorithm was used to convert the time signal to the frequency domain. To reduce the noise level of the data from the FBG and DOFSS system, the power content of the frequency spectra was estimated using Welch's power spectral density [14].

Figure 6 compares the different frequency spectra obtained from all acquisition systems located at the quarter chord line at 70% of the rotor radius.

Presented at 44th European Rotorcraft Forum, Delft, The Netherlands, 19-20 September, 2018

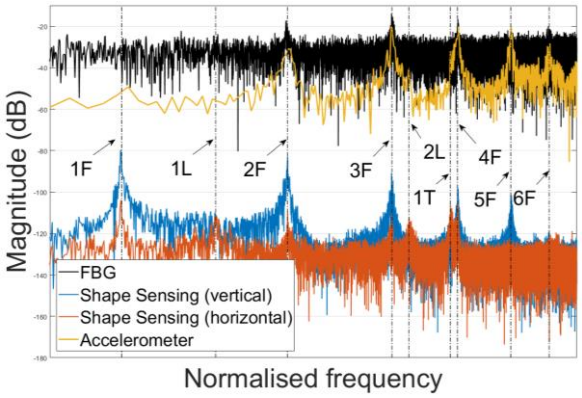

Figure 6: Comparison of frequency spectra

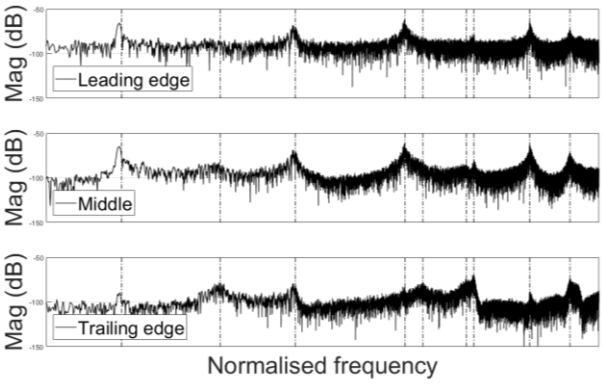

Figure 7: Frequency spectra of three FBGs in chordwise direction at 40% of rotor radius

The shape sensing data has been separated into a vertical and horizontal components, measuring out-of plane and in-plane movements. To investigate the performance and sensitivity of each system, a shaker drive force of 0.05 N was chosen. For clarity reasons the data has not been normalised.

In a frequency range of 0-100 Hz, a total of nine resonance frequencies can be observed (these are labelled as 1F *for first flapping*, 1L for *first lagging*, or 1T for *first torsion*, etc). The resonance peaks of all instrumentation systems are aligned, yet, as expected, the uniaxial accelerometers only could measure the flapping modes. The shape sensing system on the other hand was able to detect all nine resonance peaks with the capability of measuring biaxial components. Comparing the vertical and horizontal components of the shape sensing system, a coupling between the structural modes is evident. However, a significant flapping/lagging coupling of the first mode was measured, which could have been induced by some side movement of the stinger. In the data from the FBG system, only flapping modes are observed because of its position at the quarter chord line, where the horizontal distance between neutral axis and surface is close to zero. However, the 1st flapping mode is attenuated through a low signal-to-noise ratio. In order to obtain a better response, a higher drive force is required. The shape sensing system shows a much better signal-to-noise ratio despite the low drive force input, yet, the power content for higher resonance frequencies is much lower than that of the acceleration measurements.

Although the lagging and torsional modes cannot be detected by the FBGs located at the quarter chord line, a much better output is obtained from the FBGs mounted at the half chord or close to the trailing edge (see Figure 7). A shaker drive force of 1.5 N was used to obtain this output. This observation is confirmed through Eq.(2), where the surface strain is a function of the position relative to the neutral axis. Measurements at the trailing edge show that both lagging (mode 2 and 5) and torsional (mode 6) modes can be captured. This output also verifies the assumption that the neutral axis position is approximately at the quarter chord line. At the half chord position, a small power content is observable for the 1st lagging mode and the 1st torsional mode. Both the FBG and DOFSS systems capture the torsional mode by its in-plane component.

These results highlight the great potential of the DOFSS sensing system for capturing all flapping, lagging and torsional modes within the practically relevant frequency range by collecting data in one straight line along the length of the rotor blade. It also shows the importance of distributing the FBG arrays in an optimal manner over the surface in order to obtain all modes of interests.

Table 1 compares the natural frequencies determined by each of the measurement approaches. The values are normalised with respect to its first natural frequency due to proprietary reasons.

Table 1: Natural frequency

Mode no.	Mode type	Normalised frequency			
		FE	ACC	FBG	DFOSS
1	1st flap	1.00	1.00	1.00	1.00
2	1st lag	3.79	-	2.62	2.57
3	2nd fap	5.53	5.48	5.47	5.29
4	3rd flap	16.98	15.82	15.72	15.15
5	2nd lag	25.24	-	18.69	17.95
6	1st tors	31.77	-	28.88	27.21
7	4th flap	33.31	30.64	30.43	29.25
8	5th flap	57.97	53.32	52.32	49.96
9	6th flap	86.22	77.22	77.22	73.51

Presented at 44th European Rotorcraft Forum, Delft, The Netherlands, 19-20 September, 2018

The relative error e between the frequencies can be calculated as follows:

(5) $$e = \frac{f_X - f_A}{f_X}$$

Where f_X and f_A are the experimentally determined and analytical natural frequencies, respectively. Table 2 shows the calculated error between the FE model and the frequencies obtained from the GVT. The FE and accelerometer flapping frequencies are in agreement with a maximum error of 8.16%. However, the lagging frequencies have the largest error of more than 30% which could have been induced by difference between the boundary conditions used in the FE model and the test bench.

Table 2: Error between FE and experimental data

Mode no.	Mode type	Error (%)	
		FE vs ACC	FE vs FBG
1	1st flap	8.16	9.09
2	1st lag	-	-31.66
3	2nd fap	7.26	8.84
4	3rd flap	1.42	1.80
5	2nd lag	-	-21.56
6	1st tors	-	0.59
7	4th flap	0.17	0.50
8	5th flap	0.15	-0.72
9	6th flap	-2.54	-1.50

As the lagging and torsional frequency was not measured by the accelerometer, the FBG system was used as a baseline for error calculation. A comparison of the error is shown in Table 3. All natural frequencies are in agreement with a percentage error of less than 4%.

Table 3: Error between instrumentation systems

Mode no.	Mode type	Error (%)	
		FBG vs ACC	FBG vs DOFSS
1	1st flap	-1.02	3.88
2	1st lag	-	2.26
3	2nd fap	-0.93	0.55
4	3rd flap	-0.39	0.26
5	2nd lag	-	-1.08
6	1st tors	-	-2.60
7	4th flap	-0.33	0.00
8	5th flap	0.86	-0.66
9	6th flap	-1.02	-0.96

6. CONCLUSION & FURTHER WORK

This paper outlined the structural modelling of a H135 bearingless main rotor blade. Issues, such as simplifications made for the structural model or the lack of knowledge of the neutral axis position are discussed. During a GVT the rotor blade structural dynamics were collected using accelerometers and two optical fibre sensing technologies: FBG strain sensors and DOFSS. Comparing the FE model with data obtained from the FBGs, an average percentage error of 8.5 % was achieved. Natural frequencies obtain from all acquisition systems are in agreement with less than 4%.

From the data analysis a number of key benefits were identified using the novel shape sensing system compared to other commercially available technologies. These range from the ease of installation to the post processing of the collected data. No time consuming conversion from wavelength to strain or from strain to displacement is necessary. Furthermore, by only using one straight fibre optic cable, all natural frequencies of the rotor blade could be characterised with the ability of the shape sensing system to measure in-plane and out-of plane displacements. Using FBGs on the other hand, an optimal distribution of the sensor elements over the surface of the rotor blade is necessary to be able to detect lagging or torsional modes. This highlights the limitation of strain measurement as it is dependent on the position of the sensor relative to the neutral axis. Additionally, the high sensitivity of the shape sensing system was proven by comparing GVT data using the same drive force input. A much higher signal-to-noise ratio was obtained from the DFOSS system as compared to the FBGs.

To fully characterise the dynamic behaviour of the H135 rotor blade in a static environment, the displacement and strain mode shapes still have to be extracted from the frequency spectra. Finally, the instrumentation system will be applied to a fully scaled tie down test to demonstrate the capability of the developed technology in a rotating environment.

Presented at 44th European Rotorcraft Forum, Delft, The Netherlands, 19-20 September, 2018

7. REFERENCES

[1] H. Bansemir, S. Emmerling, “Fatigue Substantiation and Damage Tolerance Evaluation of Fiber Composite Helicopter Components”, RTO AVT Specialists’ Meeting on “Application of Damage Tolerance Principles for Improved Airworthiness of Rotorcraft”, (1999).

[2] K. Kampa, B. Enenkl, G. Polz, G. Roth, “Aeromechanic Aspect in the Design of the EC135”, Journal of the American Helicopter Society, Vol. 44, No. 2, pp. 83-93, (1999).

[3] H. Bansemir, R. Müller, “The EC135 – Applied Advanced Technology”, Annual Forum Proceedings – AHS International, pp. 846-861, (1997).

[4] R.L. Bielawa, “Rotary Wing Structural Dynamics and Aeroelasticity”, American Institute of Aeronautics and Astronautics, Inc., 2nd ed., (2006).

[5] N. Lawson, R. Correia, S. W. James, R.P.Tatam, et al., “Development and application of optical fibre strain and pressure sensors for in-flight measurements”, Meas. Science and Tech., 27, Art. 104001, (2016).

[6] S. J. Buggy, S.W. James, S. Staines, R. P. Tatam, et al., “Railway track component condition monitoring using optical fibre Bragg grating sensors”, Meas. Science and Tech., 27, Art. 055201, (2016).

[7] R. M. Groves, E. Chehura, W. Li, R.P.Tatam, et al., “Surface strain measurement: a comparison of speckle shearing interferometry and optical fibre Bragg gratings with resistance foil strain gauges”, Meas. Science and Tech., 18, pp. 1175-1184, (2007).

[8] A. Cusano, A. Cutolo and J. Albert, “Fiber Bragg Grating Sensors: Recent Advancements, Industrial Applications and Market Exploitation” Bentham Science Publishers (2018).

[9] M.J. Nicolas, R. W. Sullivan, W. L. Richards, “Large Scale Applications Using FBG Sensors: Determination of In-Flight Loads and Shape of a Composite Aircraft Wing” Aerospace 3, 18 (2016).

[10] T. Kissinger, E. Chehura., S.E. Staines, S.W. James, R.P. Tatam, “Dynamic fiber-optic shape sensing using fiber segment interferometry,” J. Lightwave Technol., 36, pp. 917-925, (2018).

[11] T. Kissinger, T.O.H. Charrett, R.P. Tatam, “Range-resolved interferometric signal processing using sinusoidal optical frequency modulation,” Opt. Express 23, pp. 9415-9431, (2015).

[12] T. Kissinger, R. Correia, T.O.H. Charrett, S.W. James, R.P. Tatam, “Fiber segment interferometry for dynamic strain measurements,” J. Lightwave Technol., 34, pp. 4620-4626, (2016).

[13] Y.J. Rao, “In-fibre Bragg grating sensors”, Meas. Sci. Technol. 8, pp. 355-375, (1997).

[14] P. Welch, “The Use of Fast Fourier Transform for the Estimation of Power Spectra: A Method Based on Time Averaging Over Short, Modified Periodograms”, IEEE Transactions on audio and electoacoustics, Vol 15, (2), pp. 70-73, (1967).

Presented at 44th European Rotorcraft Forum, Delft, The Netherlands, 19-20 September, 2018